International Journal of Applied Mathematics

Volume 38 No. 1s, 2025

ISSN: 1311-1728 (printed version); ISSN: 1314-8060 (on-line version)

PERTURBATION HEAT TRANSFER IN MULTI NANOFLUIDS- FILLED CONTAINER WITH IRREGULAR TEMPERATURE: MAXWELL VS MODIFIED MAXWELL

[1]S. S. Ananthan, [2]S. Sureshkumar, [3]Dr. Hari Jyothula, [4]Dr. J. Leo Amalraj, [5]Madhava Rao Chunduru

[1]Department of Mathematics, Erode Sengunthar Engineering College, Thudupathi, Erode - 638057, India

[2]Department of Mathematics, Saveetha Engineering College, Chennai-602105, India

[3]Assistant Professor, Computer Science and Engineering, Aditya University, Surampalem

[4]Associate professor, Department of Mathematics, RMK College of Engineering and Technology, Puduvoyal, Thiruvallur District, Tamilnadu, India

[5]Associate Professor, Department of Computer Science and Engineering, Koneru Lakshmaiah Educational Foundation Vaddeswaram, Guntur District, Ap, India.

ananthmathsesec@gmail.com, skmaths0704@gmail.com, dr.jyothulahari@gmail.com, leoamalraj@rmkcet.ac.in, cmadhavarao@kluniversity.in

Abstract

Mixed convection in a heat generating nanofluid filled square enclosure partially heated from below with uniform and non-uniform heating is numerically investigated. The vertical walls and the remaining portion of the bottom wall are insulated while the top wall is cooled with uniform velocity. The governing equations are solved by finite volume method on an uniformly staggered grid. The results are discussed for different combination of physical parameters, namely, Reynolds number, Grashof number, the non-dimensional perturbation (S) and solid volume fraction. It has been observed that the rate of heat transfer increases with higher Reynolds number, Grashof number, and solid volume fraction. Uniform heating greatly boosts the overall heat transfer efficiency in contrast to non-uniform heating. The non-dimensional perturbation at 2 has a more significant effect on the temperature distribution than the other cases. The modified Maxwell model demonstrates a higher heat transfer rate than the standard Maxwell model.

Keywords: Perturbation Heat generation; Multi Nanofluid; Mixed convection; Nonuniform heating, Maxwell vs Modified Maxwell

Nomenclature

g gravitational acceleration, m/s^2

Received: July 18, 2025

International Journal of Applied Mathematics

Volume 38 No. 1s, 2025

ISSN: 1311-1728 (printed version); ISSN: 1314-8060 (on-line version)

Gr	Grashof number, $\frac{g\beta\Delta\theta H^3}{\nu_f^2}$
L	enclosure length, m
h_{nl}	thickness of nano-layer, nm
k_f	thermal conductivity of the fluid, W/m K
k_s	thermal conductivity of the solid, W/m K
Nu_{avg}	average Nusselt number
Nu	local Nusselt number
P	pressure
Pr	Prandtl number, $\frac{\nu_f}{\alpha_f}$
Q_0	heat generation or absorption coefficient
r_s	radius of nanoparticles, nm
Re	Reynolds number, $\frac{U_p L}{\nu_f}$
Ri	Richardson number, Gr/Re^2
S	non-dimensional perturbation in the form of internal heat generation
T	dimensionless temperature, $\frac{\theta-\theta_c}{\theta_h-\theta_c}$
U, V	dimensionless velocities in X- and Y-direction respectively
U_0	lid velocity, $\mathrm{m/s}$
U_c	dimensionless velocity in X-direction at mid-plane of the cavity
u, v	velocities in x - and y-direction respectively
$\underset{\rightarrow}{V_c}$	dimensionless velocity in Y-direction at mid-plane of the cavity
$\vec{V}$	dimensionless velocity vector
X, Y	dimensionless Cartesian coordinates
x, y	Cartesian coordinates

Received: July 18, 2025

Greek symbols

α	effective thermal diffusivity, m^2/s
β_f	coefficient of thermal expansion of fluid, K^{-1}
β_f	coefficient of thermal expansion of solid, K^{-1}
$\Delta\theta$	temperature difference
θ	temperature $\,^{\circ}\mathrm{C}$
μ	effective dynamic viscosity $\mathrm{kg/ms}$
ν	effective kinematic viscosity, m^2/s
ρ	fluid density $\mathrm{kg/m}^3$
χ	solid volume fraction
η	ratio of thermal conductivity of nano-layers

Subscripts

avg	average
c	cold wall
eff	effective
eq	equivalent
f	fluid
h	hot wall
nf	nanofluid
nl	nano-layer
s	solid

1. Introduction

Mixed convection, characterized by the interaction of natural and forced convection mechanisms to facilitate heat transfer, is crucial in many applications. In particular, the behavior of a pure fluid within a cavity with a moving wall has been extensively researched in the field of heat and mass transfer due to its diverse applications. Ji et al. [1] explored mixed convection in a cavity where the lid slides along the top. Their study has revealed that when Richardson

Received: July 18, 2025

Volume 38 No. 1s, 2025
ISSN: 1311-1728 (printed version); ISSN: 1314-8060 (on-line version)

number is less than one, the temperature in the bulk of the cavity becomes uniform when the system reaches steady state. Sharif [2] investigated combined convection in thin, slanted cavities with moving hot and cold walls at the top and bottom of the cavity, respectively. The findings demonstrated that the average Nusselt number increases moderately at $\mathrm{Ri} = 0.1$ and significantly at $\mathrm{Ri} = 10$ as the cavity's inclination angle increases. Investigations into combined convection in chambers featuring various thermal boundary conditions and different moving lids have been documented in studies [3-8].

The thermal conductivity of fluids is essential in the development of energy-efficient heat exchange systems. Unfortunately, conventional heat transfer fluids exhibit relatively low thermal conductivity. The growing global competition drives the need for advanced fluids with superior thermal conductivity. Nanofluids, a revolutionary class of fluids, are produced by introducing nanoscale particles into conventional fluids. This innovative approach promises enhanced thermal properties. The feasibility of the concept of high-thermal-conductivity nanofluids has been exhibited by Masuda et al. [9]. Choi [10] made an analysis on enhancing thermal conductivity of fluids with nanoparticles. Initially, Maxwell [11] pioneered the development of a model that predicts the thermal conductivity of mixtures with embedded solid particles. He had found that spherical shape of particles provide the enhanced thermal conductivity. Kumar and Prasad [12] applied a single-phase thermal dispersion model to examine the flow and thermal characteristics of nanofluids. Their results showed that the potential of a nanofluid for heat transfer applications depends on the proper modeling of convective transport properties. Interesting investigations on thermal transfer of nanofluids in a lid moving chambers can be found in [12-18].

The above reviewed studies fall into two categories: the first investigates mixed convection $[1-8]$, while the second examines the impact of nanofluids [12-18]. All kind of the above works cited previously have their own significance in the literature due to their applications. Hence, any numerical approach involving mixed convection, internal heat generation or absorption, uniform or non-uniform heating, partial heating and nanofluids would be a special kind of interest to study. The literature has not yet addressed the problem of nanofluid-mixed convection heat transfer in a cavity subject to perturbations such as internal heat generation or absorption, combined with uniform and non-uniform heating along part of the bottom wall. Hence, the present investigation focuses on studying mixed convection in a heat-generating nanofluid-filled square enclosure that is partially heated from below, considering both uniform and non-uniform heating.

2. Mathematical Analysis

In this study, a two-dimensional square cavity of size L, filled with Cu-water nanofluid under steady-state conditions is considered, as depicted in Fig.1. The top boundary moves at a constant speed U_0 in the left-to-right direction and is held at a constant temperature θ_c. Part of

Received: July 18, 2025

Volume 38 No. 1s, 2025

ISSN: 1311-1728 (printed version); ISSN: 1314-8060 (on-line version)

the bottom wall is maintained at a uniform and non-uniform temperature $\theta_h(\theta_h > \theta_c)$, with the remaining sections of the bottom wall and both side walls being insulated. The enclosure contains a Newtonian, incompressible nanofluid that exhibits laminar flow. It is treated as a dilute mixture of solid and liquid phases, containing a uniform volume fraction of five types of nanoparticles in water. It is assumed that the base fluid and the nanoparticles are thermally balanced and flow at the same velocity. As given in Table 1[13], [14], based on Boussinesq's approximation, the thermophysical properties of the nanofluid are assumed constant, with the exception of the density. No chemical reactions are presumed between the nanoparticles and the base fluid.

Table 1 Thermophysical properties of water and nanoparticles [13], [14].

	$\rho(\text{kgm}^{-3})$	$C_p(\text{Jkg}^{-1}\ \text{K}^{-1})$	$k(\text{Wm}^{-1}\ \text{K}^{-1})$	$\beta \times 10^{-5}(\ \text{K}^{-1})$
H_2O	997.1	4179	0.613	21
Cu	8933	385	401	1.67
Ag	10500	235	429	1.89
CuO	6320	531.8	76.5	1.8
Al_2O_3	3970	765	40	0.85
TiO_2	4250	686.2	8.9538	0.9

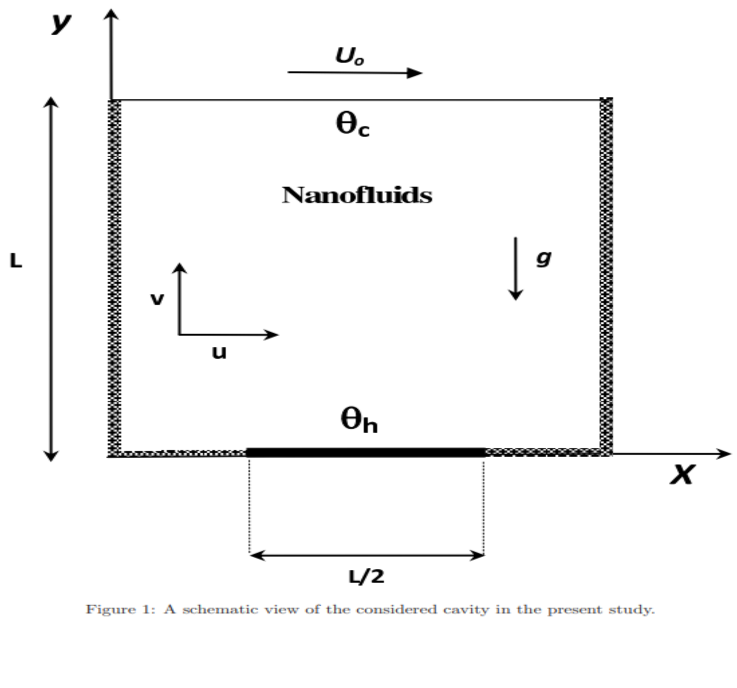

Figure 1: A schematic view of the considered cavity in the present study.

Received: July 18, 2025

Volume 38 No. 1s, 2025

ISSN: 1311-1728 (printed version); ISSN: 1314-8060 (on-line version)

The governing equations for these consideration of the system can be written as follows [13], [14]

$$\frac{\partial u}{\partial x}+\frac{\partial v}{\partial y}=0 \tag{1}$$

$$u\frac{\partial u}{\partial x}+v\frac{\partial u}{\partial y}=-\frac{1}{\rho_{nf}}\frac{\partial p}{\partial x}+\frac{\mu_{eff}}{\rho_{nf}}\nabla^2 u \tag{2}$$

$$u\frac{\partial v}{\partial x}+v\frac{\partial v}{\partial y}=-\frac{1}{\rho_{nf}}\frac{\partial p}{\partial y}+\frac{\mu_{eff}}{\rho_{nf}}\nabla^2 v+\frac{1}{\rho_{nf}}\left[\chi\rho_{s,0}\beta_s+(1-\chi)\rho_f\beta_f\right]g(\theta-\theta_c) \tag{3}$$

$$u\frac{\partial \theta}{\partial x}+v\frac{\partial \theta}{\partial y}=\alpha_{nf}\nabla^2\theta+\alpha_{nf}\frac{Q_0}{\left(\rho C_p\right)_{nf}}(\theta-\theta_c) \tag{4}$$

By employing the dimensionless parameters listed below, the above equations can be converted into their non-dimensional form:

$$X=\frac{x}{L},Y=\frac{y}{L},U=\frac{u}{U_0},V=\frac{v}{U_0},T=\frac{\theta-\theta_c}{\theta_h-\theta_c},Gr=\frac{g\beta\Delta\theta L^3}{v_f^2},Ri=\frac{Gr}{Re^2}$$

The dimensionless form of governing equations is:

$$\vec{\nabla}\cdot\vec{V}=0 \tag{6}$$

$$\vec{V}\cdot\vec{\nabla}U=-\frac{\partial P}{\partial X}+\frac{1}{Re}\frac{\mu_{eff}}{v_f\cdot\rho_{nf}}\nabla^2 U \tag{7}$$

$$\vec{V}\cdot\vec{\nabla}V=-\frac{\partial P}{\partial Y}+\frac{1}{Re}\frac{\mu_{eff}}{v_f\cdot\rho_{nf}}\nabla^2 V+\frac{(\rho\beta)_{nf}}{\rho_{nf}\beta_f}RiT \tag{8}$$

$$\vec{V}\cdot\vec{\nabla}T=\frac{\alpha_{nf}}{\alpha_f}\frac{1}{Pr\cdot Re}\nabla^2 T+\frac{\alpha_{nf}}{\alpha_f}\frac{S}{\mathrm{PrRe}T} \tag{9}$$

where S is a factor representing the disturbance from internal heat generation and defined by $S=1.25\times[\mathrm{rand}(0,1)-0.5]$ where $\mathrm{rand}(0,1)$ is a random number generator. The associated boundary conditions to the equations (6) to (9) are as follows.
$U=1,V=0,T=0\ (Y=1)$
$U,V=0,T=1$ or $T=\sin(\pi X)\ (Y=0)$

$U,V=0,\frac{\partial T}{\partial X}=0(X=0,1)$.
The properties of the nanofluids are given in Table 2 [13], [14].
The rate of heat transfer is determined by the local (Nu) and average Nusselt (Nu_{avg}) numbers as given below.

Received: July 18, 2025

$$Nu = -\frac{k_{eff}}{k_f}\frac{\partial T}{\partial Y} \tag{11}$$

$$Nu_{\text{avg}} = \int_0^1 NudX. \tag{12}$$

The modified Maxwell [19]model for the effective thermal conductivity of the nanofluid, k_{eff}, for spherical nanopartilces is

$\frac{k_{eff}}{k_f} = \frac{(k_{eq}+2k_f)+2(k_{eq}-k_f)(1+\sigma)^3\chi}{(k_{eq}+2k_f)-(k_{eq}-k_f)(1+\sigma)^3\chi}$.

where, $\sigma = h_{nl}/r_s$ and the equivalent thermal conductivity k_{eq} of nanoparticles and their layers is given by

$\frac{k_{eq}}{k_s} = \eta\frac{2(1-\eta)+(1+\sigma)^3(1+2\eta)}{-(1-\eta)+(1+\sigma)^3(1+2\eta)}$.

where, $(\eta = k_{nl}/k_s)$. Yu and Choi [19] experimentally proved the results of the modified Maxwell model for the value of $h_{nl} = 2nm, r_s = 3nm$ and $k_{nl} = 100k_f$ and the same values are assumed in this study also.

Table 2 Applied formulae for the nanofluid properties [13], [14].

Nanofluid properties	Applied model
Density	$\rho_{nf,0} = (1-\chi)\rho_{f,0} + \chi\rho_{s,0}$
Thermal diffusivity	$\alpha_{nf} = \frac{k_{\text{eff}}}{(\rho C_p)_{nf,0}}$
Heat capacitance	$(\rho C_p)_{nf} = (1-\chi)(\rho C_p)_f + \chi(\rho C_p)_s$
Dynamic viscosity	$\mu_{eff} = \frac{\mu_f}{(1-\chi)^{2.5}}$
Thermal expansion coefficient	$(\rho\beta)_{nf} = \chi\rho_s\beta_s + (1-\chi)\rho_f\beta_f$

3.Numerical Technique and Validation

3.1 Numerical Method

The non-dimensional equations (6)-(9), subject to boundary conditions, are solved using the finite volume method on a uniform staggered grid configuration, utilizing the SIMPLE algorithm of Patankar [20]. To mitigate numerical diffusion in the convective terms for both momentum and energy equations, the third-order accurate deferred QUICK scheme by Hayase

Volume 38 No. 1s, 2025

ISSN: 1311-1728 (printed version); ISSN: 1314-8060 (on-line version)

et al. [21] is applied. By integrating over each control volume, the governing equations are transformed into algebraic equations. TDMA line-by-line method is used to solve the discretized momentum and pressure correction equations. Successively refined uniform grids, ranging from 21×21 to 101×101, were used for the grid independence test with $Ri = 1$ and $\chi = 0.06$. It was observed that a 61×61 grid is sufficient to ensure accuracy and minimize computational time.

3.2 Code Validation

The numerical model was validated by comparing the results with those of Iwatsu et al. [22] for $Re = 400, Gr = 10^6$ and $\mathrm{Pr} = 0.71$. Fig. 2(a) displays the local Nusselt number, showing a strong correlation between the present simulation results and those of Iwatsu et al. Validation of the present computational code was further performed by assessing the impact of viscosity model uncertainties for Al_2O_3-water nanofluid on mixed convection simulations, following the work of Mahmoodi et al. [23]. Fig. 2(b) presents a comparison of the dimensionless vertical velocity component for $Ri = 100$ with varying nanoparticles volume fractions, showing excellent agreement. This confirms the accuracy and reliability of the code in addressing the current problem.

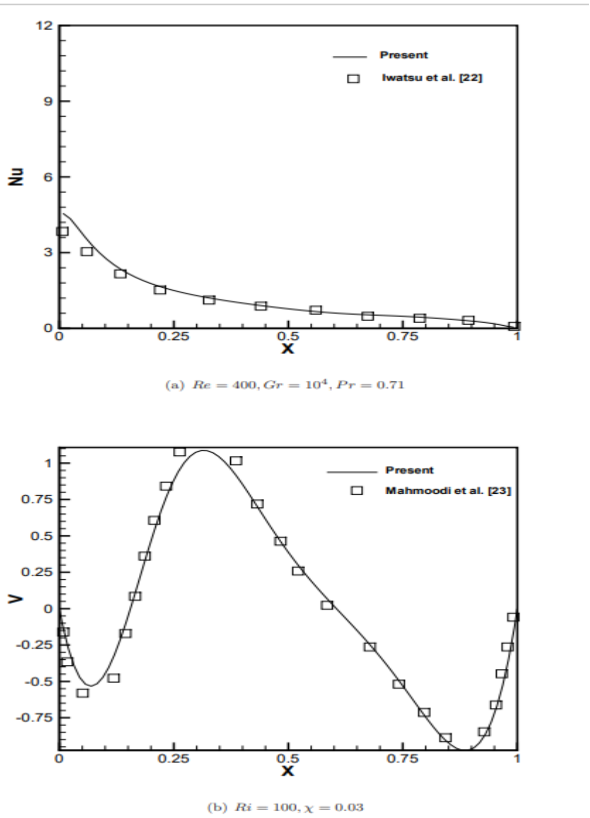

Figure 2: Validation of the present code with the results of (a) Iwatsu et al. [22] and (b) Mahmoodi et al. [23].

Received: July 18, 2025

International Journal of Applied Mathematics

Volume 38 No. 1s, 2025

ISSN: 1311-1728 (printed version); ISSN: 1314-8060 (on-line version)

4. Results and Discussion

In the present work, the numerical results for combined convection heat transfer of a heat-generating nanofluid in a square lid-driven cavity partially heated from below with uniform and non-uniform heating, and filled with water-base nanofluids containing various nanoparticles such as $\mathrm{Ag}, \mathrm{Al_2O_3}, \mathrm{Cu}, \mathrm{CuO}, \mathrm{TiOO_2}$ are discussed. In the cavity, a part of bottom wall is uniformly and non-uniformly heated while the other parts of bottom wall and the two vertical walls are insulated. Cold top wall is moving with uniform velocity. The effect of physical parameters on the resulting streamlines, isotherms, velocity profiles and both the Nusselt number and the average Nusselt number has been analyzed. Throughout the investigation, the Prandtl number $\mathrm{Pr} = 6.2$ is fixed. The results of this parametric study are revealed in Figs. 3-13 for a range of Reynolds number ($100 \leq Re \leq 1000$), Grashof number ($10^2 \leq Gr \leq 10^6$), the non-dimensional perturbation(S) in the form of internal heat generation and solid volume fraction ($0 \leq \chi \leq 0.06$).

Fig. 3 depicts isotherms and streamlines for various Reynolds number ($100 \leq Re \leq 1000$) when $Gr = 10^4$ and $\chi = 0.06$ are fixed. The figure shows that the natural convection and forced convection are in a comparable level. It is displayed that the temperature contour maps of fluid are clustered close to a part of bottom wall Leading to significant temperature variations in that area while increasing Reynolds number. The temperature gradients are minimal in the rest of the enclosure due to the vigorous effects of the shear-driven circulations. Driven by the top wall's motion, the fluid flow features a large clockwise rotating eddy filling the cavity, with counterclockwise rotating eddies forming at the bottom corners. As can be seen from Fig. 3 (a), Near the bottom corners, minor eddies are present when $Re = 100$. An intriguing observation is that the minor eddies expand in size as the Reynolds number becomes larger. In Fig.4, the discussion is based on fixed values of $Re = 100$ and $\chi = 0.06$, and varying Grashof number ($10^2 \leq Gr \leq 10^6$). In Fig. 4(a), the isotherms appear to be concentrated along the bottom and left walls. With a further rise in Gr, the isotherms compress more significantly, and a distinct thermal boundary layer forms. Non-uniform heating of the bottom wall produces similar effects. It is revealed that convection plays a dominant role in heat transfer irreapective of the thermal source. At $Gr = 10^2$, a primary recirculation is created near the top right corner which occupies the most the cavity and a secondary recirculation is created at the bottom of the right corner while another small recirculation is formed at bottom of the left corner. When the Grashof number is increased to 10^5 and 10^6, the primary recirculation in the flow is gradually moved to the region at the center of the cavity (Fig. 4(b)-4(c)) and the secondary recirculation of both bottom corners is disappeared. It is discovered that the flow behavior is essentially established in the enclosure with the change in Grashof number. The effect of buoyancy is significant throughout the cavity while increasing the Grashof number.

Fig. 5 illustrates the isotherms and streamlines for the non-uniform heating case with various values of solid volume fraction while the ($Gr = 10^6$) and ($Re = 10^2$) are fixed. Clear

International Journal of Applied Mathematics

Volume 38 No. 1s, 2025

ISSN: 1311-1728 (printed version); ISSN: 1314-8060 (on-line version)

distinctions in the isotherm contour plots between the cases of $\chi = 0$ (pure water) and $\chi = 0.06$ (nanofluid) are confirmed in Fig. 5. Fig. 5(a) shows the primary vortex dissipating in the cavity's center, resulting in the formation of two secondary vortices when ($\chi = 0$). Consequently, the streamlines become distorted, and a multi-cellular flow pattern develops. When the buoyancy effect is significant, the presence of nanoparticles in Fig. 5(b) leads to an increase in circulation strength compared to Fig. 5(a), causing the fluid to move faster in the enclosure and the two secondary vortices to vanish. It is found that for $Re = 100, Gr = 10^6$ and $\chi = 0.06$, the flow field inside the cavity increases and always changes remarkably with respect to the solid volume fraction of nanoparticles.

Fig. 6 shows the effect of solid volume fraction on the horizontal velocity distribution for various ($100 \leq Re \leq 1000$) and ($10^2 \leq Gr \leq 10^6$). The buoyancy effect is eclipsed by the sliding lid's mechanical effect in Fig. 6(a), leading to a minimal response in flow intensity to changes in solid volume fraction. In Fig. 6 (b), the increase of both Grashof number and solid volume fraction establish the flow field inside the cavity and augment the strength of buoyancy. So this causes the horizontal centerline velocity components to increase. Fig. 7 displays the effects of solid volume fraction, Re and Gr on the vertical velocity component at mid of the chamber, respectively. This results show that upward flow and downward flow are symmetric with respect to center of the cavity. It is predicted from this Fig. 6-7 that for $Re = 100, Gr = 10^6$ and $\chi = 0.06$, the buoyancy effect and the solid volume fraction of nanoparticles give remarkable changes in the intensity of the flow field. Meanwhile, it must be noted that the horizontal velocity component is more responsive to lid-driven flow than the vertical velocity component.

Fig. 8 illustrates the variations of local Nusselt numbers on a part of bottom wall for various Re, χ, and for fixed ($Gr = 10^4$). According to the figure, the Nusselt number varies based on solid volume fraction for various Reynolds number on both the thermal source. For $Gr/Re^2 = 1$, both forced and natural convection affect on flow field and heat transfer over the surface of the cavity. It can be understood from this Fig. 8(a) that for $Re = 100$, The Nusselt number exhibits near-linearity within half of the cavity and experiences a rise after certain thresholds are crossed. Nusselt number increases first and then decreases for all solid volume fractions as the vigorous effects of lid motion has the tendency to fast up the movement of the fluid which is depicted in Fig. 3(b-c). It is due to anticlockwise rotating secondary eddies at corners of the bottom surface. In Fig. 8(b), the curves depicted for the Nusselt numbers against X produce a sinusoidal type approximately. It can be concluded from this figure that the distribution of temperature on the surface plays a direct role in influencing local heat transfer.. The variations of local Nusselt numbers on the partially heated bottom wall are exhibited in Fig. 9 for various Grashof number ($10^2 \leq Gr \leq 10^6$) and solid volume fraction ($0 \leq \chi \leq 0.06$), and for fixed Reynolds number ($Re = 10^2$). When natural convection prevails, there is a significant change in heat transfer on the heated wall while increasing the solid volume fraction ($0 \leq \chi \leq 0.06$). The fact is revealed in this Fig. 9(a-b).

Received: July 18, 2025

International Journal of Applied Mathematics

Volume 38 No. 1s, 2025

ISSN: 1311-1728 (printed version); ISSN: 1314-8060 (on-line version)

The variations of Nu_{avg} for various Re, Gr, and χ with both heating are performed in Fig. 10. Inspection of Fig. 10(a-b) shows that the Nu_{avg} have been increased significantly with an increase in the χ, Re and Gr. In addition, the Nu_{avg} increases almost linearly with χ for mixed convection, forced convection and free convection. It can be understood with isotherms and local Nusselt numbers discussed in the previous figures. The average Nusselt number is icreased markedly for high Richardson number and low Richardson number. Also, it must be noted that the uniform heating is more responsive to transfer heat than the non-uniform heating.

Fig. 11 displays Nu_{avg} for perturbation internal heat generation for various solid volume fraction $(0 \leq \chi \leq 0.06)$. The standard case involves a random perturbation $S = 1.25 \times [\text{rand}(0,1) - 0.5]$, and supplementary cases are analyzed with perturbations of $S/2$ and $2S$. The basic case for comparison has the random perturbation given by , and two additional cases, one with perturbation $2S$ and the other with perturbation, were calculated. The non-dimensional perturbation at $2S$ gives the better effect on the temperature distribution than remaining cases. Fig. 12 depicts the Nu_{avg} for the different type of nanoparticles with various solid volume fractions. Since the average Nusselt number depends strongly on the density of nanoparticles, the Nu_{avg} is increased with respect to the solid volume fractions. But, the better heat transfer is obtained for water- CuO nanofluid compared with water- Al_2O_3, water- Ag , water- Cu and waterTiO_2. Fig. 13 presents the Nu_{avg} for the two models (Maxwell and Modified Maxwell model) at the hot lid of the enclosure for various Reynolds number ($100 \leq Re \leq 1000$) with different type of solid volume fraction $(0 \leq \chi \leq 0.06)$. Both models enhance the heat transfer with increased Re and χ. However, the results of Modified Maxwell model is more responsive to transfer heat than the Maxwell model.

Received: July 18, 2025

International Journal of Applied Mathematics

Volume 38 No. 1s, 2025

ISSN: 1311-1728 (printed version); ISSN: 1314-8060 (on-line version)

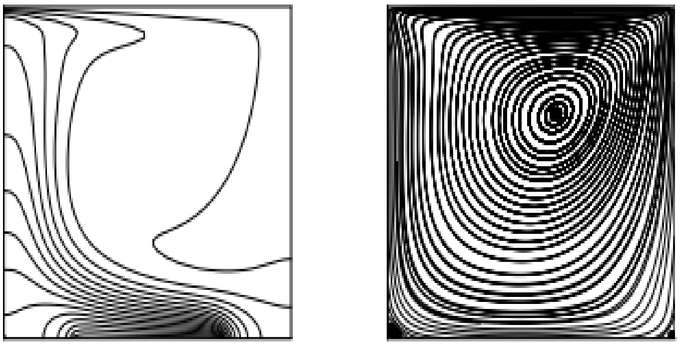

(a) $Re = 100$

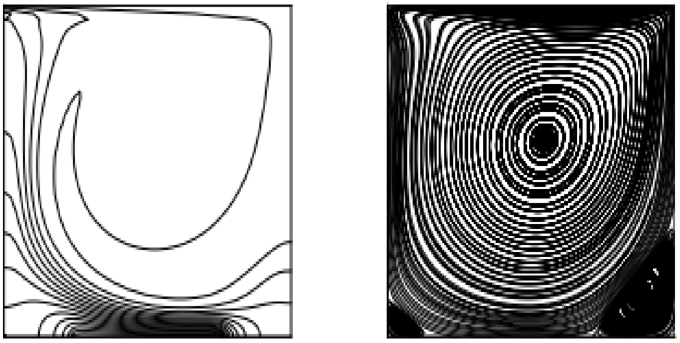

(b) $Re = 400$

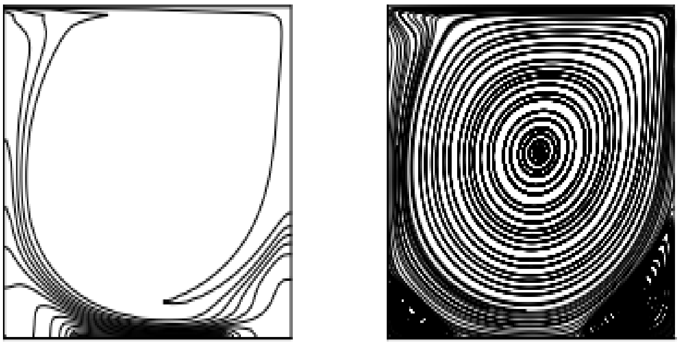

(c) $Re = 1000$

Figure 3: Isotherms (left) and Streamlines (right) for $Gr = 10^4$ and $\chi = 0.06$ (uniform heating).

Received: July 18, 2025

International Journal of Applied Mathematics

Volume 38 No. 1s, 2025

ISSN: 1311-1728 (printed version); ISSN: 1314-8060 (on-line version)

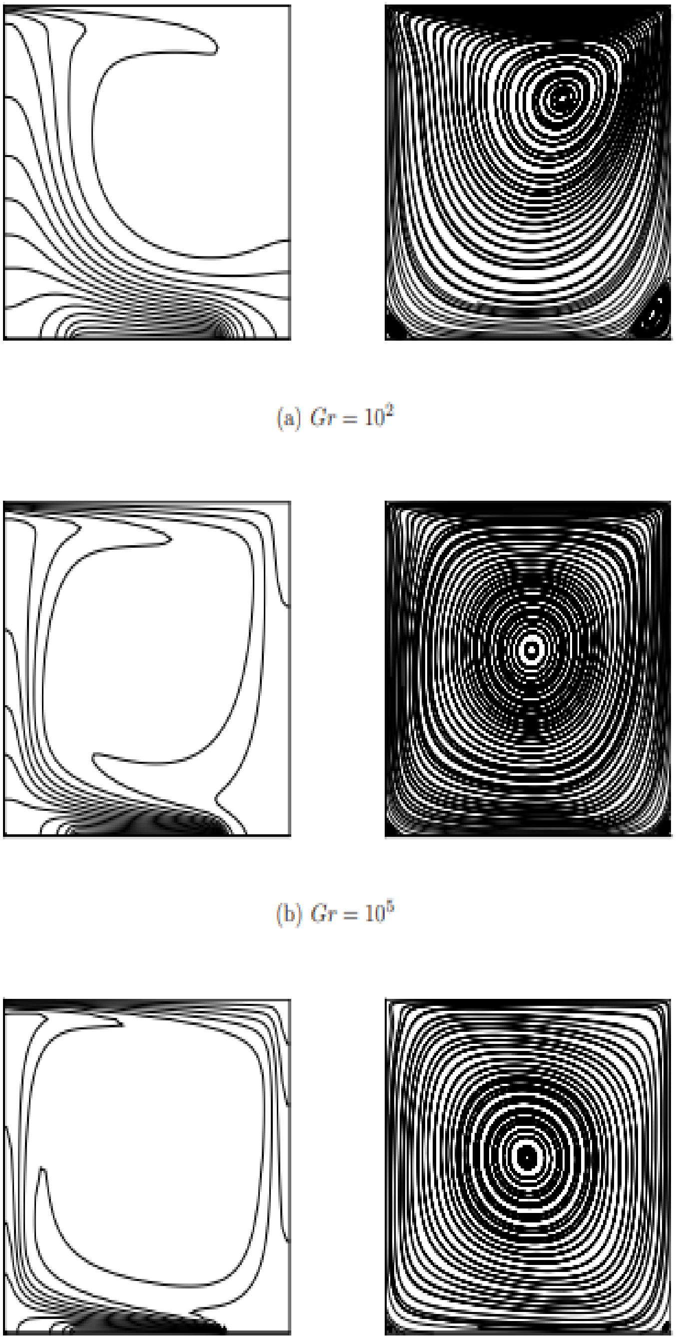

(a) $Gr = 10^2$

(b) $Gr = 10^5$

(c) $Gr = 10^6$

Figure 4: Isotherms (left) and Streamlines (right) for $Re = 100$ and $\chi = 0.06$ (uniform heating).

International Journal of Applied Mathematics

Volume 38 No. 1s, 2025

ISSN: 1311-1728 (printed version); ISSN: 1314-8060 (on-line version)

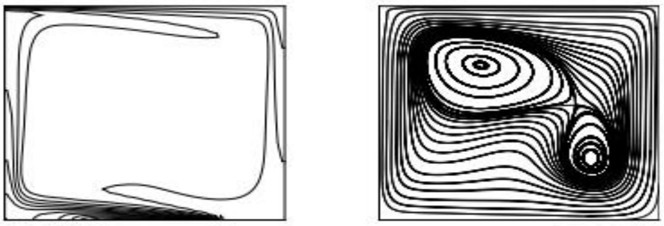

(a) $\chi = 0$

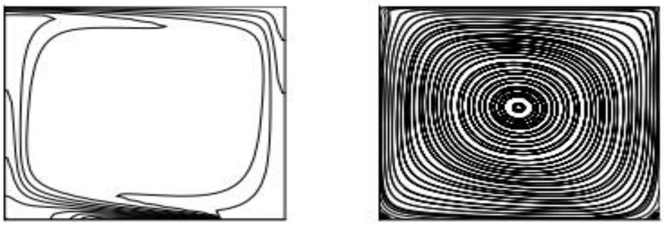

(b) $\chi = 0.06$

Figure 5: Isotherms (left) and Streamlines (right) for $Re = 100$ and $Gr = 10^6$ (non-uniform heating).

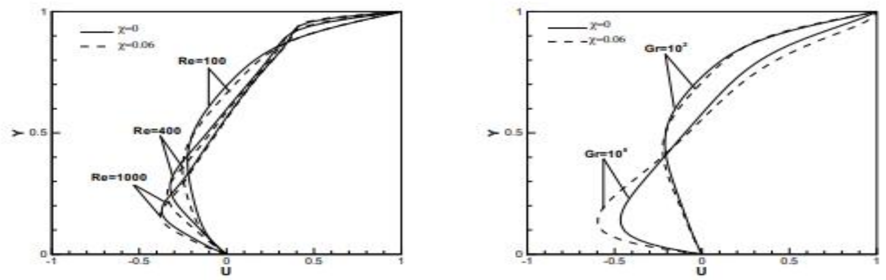

(a) (b)

Figure 6: U-Velocity profiles at mid-plane of the cavity for (a) $Gr = 10^4$ and (b) $Re = 100$ (uniform heating).

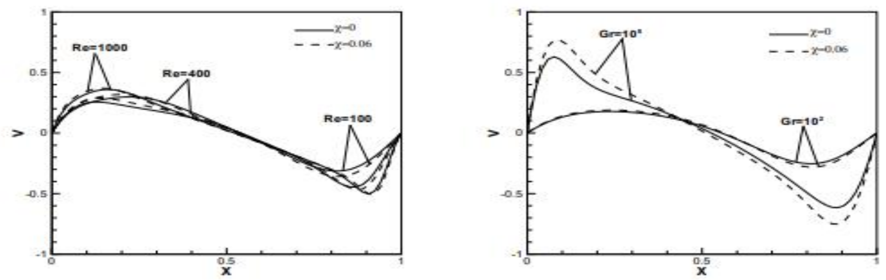

(a) (b)

Figure 7: V-Velocity profiles at mid-plane of the cavity for (a) $Gr = 10^4$ and (b) $Re = 100$ (uniform heating).

Received: July 18, 2025

International Journal of Applied Mathematics

Volume 38 No. 1s, 2025

ISSN: 1311-1728 (printed version); ISSN: 1314-8060 (on-line version)

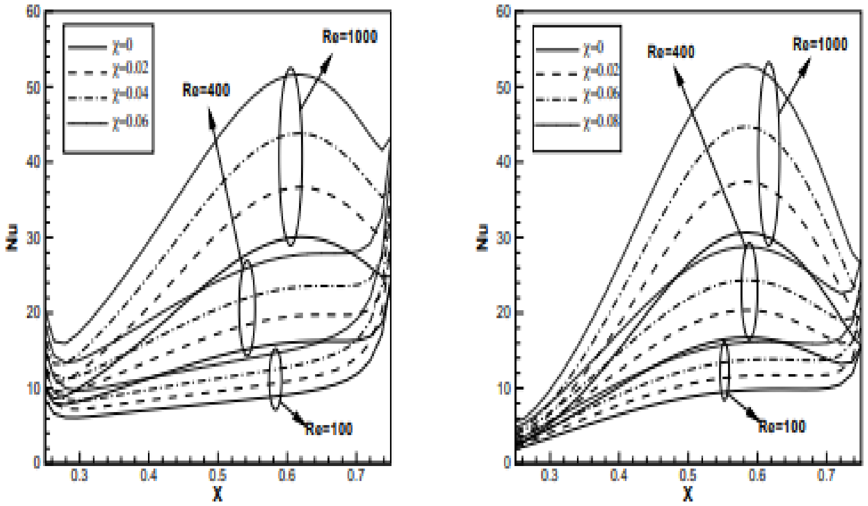

(a) (b)

Figure 8: Local Nusselt number for $Gr = 10^4$ with uniform heating (a) and non-uniform heating (b).

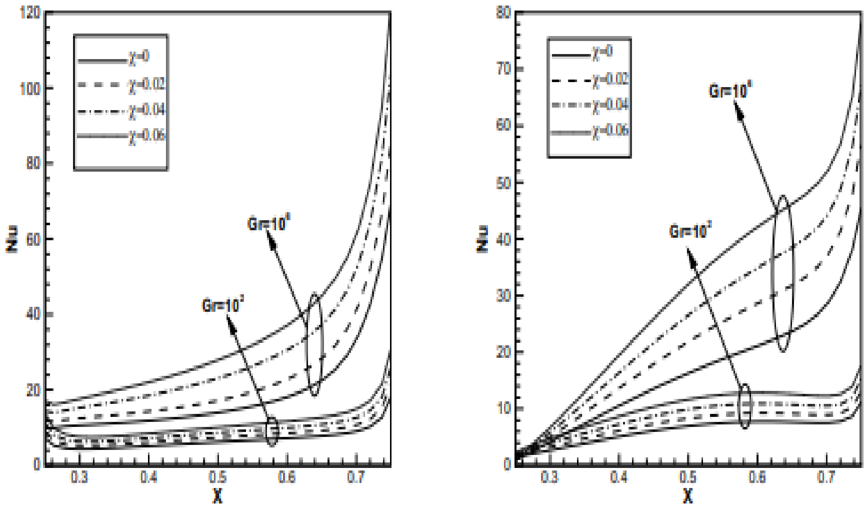

(a) (b)

Figure 9: Local Nusselt number for $Re = 100$ with uniform heating (a) and non-uniform heating (b).

Received: July 18, 2025

International Journal of Applied Mathematics

Volume 38 No. 1s, 2025

ISSN: 1311-1728 (printed version); ISSN: 1314-8060 (on-line version)

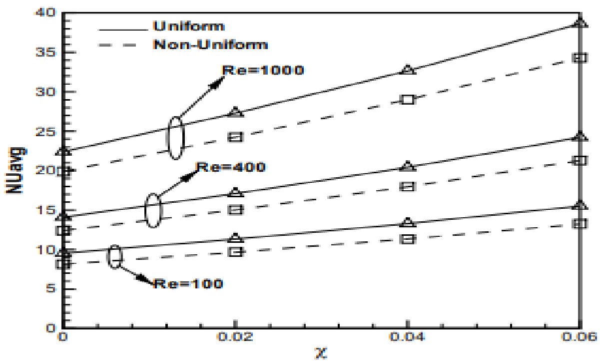

(a)

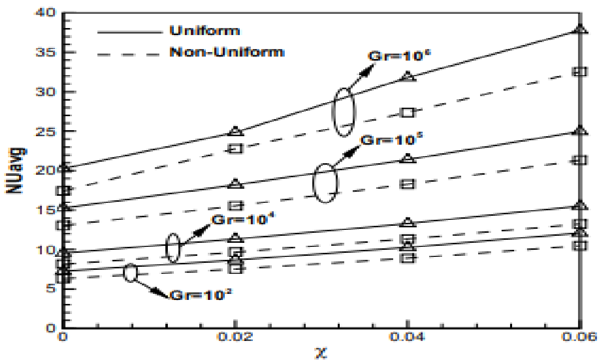

(b)

Figure 10: Average Nusselt number for (a) $Gr = 10^4$ and (b) $Re = 100$.

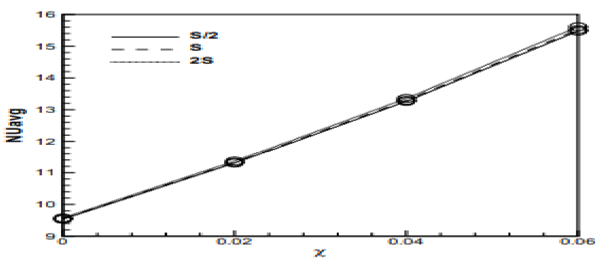

Figure 11: Average Nusselt number for perturbation internal heat generation.

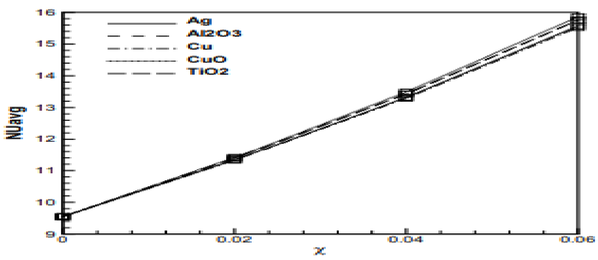

Figure 12: Average Nusselt number for different nanofluids.

Received: July 18, 2025

ISSN: 1311-1728 (printed version); ISSN: 1314-8060 (on-line version)

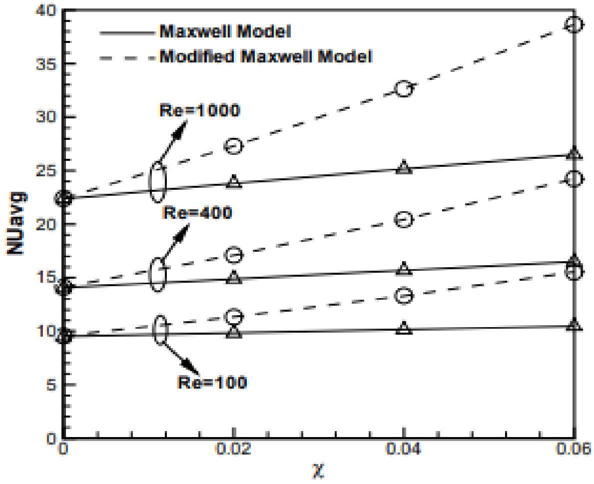

Figure 13: Comparison of average Nusselt number between Maxwell and modified Maxwell model.

5. Conclusions

Computation of nanofluid-mixed convection is carried out using modified Maxwell model in a square lid-driven cavity partially heated from below with uniform and nonuniform heating, and internal heat generation. From this investigation, the following conclusions have been drawn.

- For $Re = 100, Gr = 10^6$ and $\chi = 0.06$, there is a remarkable change on both streamlines and isotherms with uniform and non-uniform heating as the solid volume fraction of nanoparticles and buoyancy effect have the major role on the intensity of the flow field.
- The influence of lid-driven flow on horizontal velocity is greater than its effect on vertical velocity.
- The uniform heating on a part of bottom wall have greater influence on heat transfer than non-uniform heating.
- The non-dimensional perturbation at $2S$ gives the better effect on the temperature distribution than remaining cases.
- The significant heat transfer enhancement can be drawn due to the presence of nanoparticles. But, the better heat transfer is obtained for water- CuO nanofluid compared with water- Al_2O_3, water- Ag , water- Cu and water- TiO_2.

References

[1] T.H. Ji, S.Y. Kim, J.M. Hyun, Transient mixed convection in an enclosure driven by a sliding lid, Int. J. Heat Mass Transfer 43 (2007) 629-638. DOI: 10.1007/s00231-006-0113-y.

Received: July 18, 2025

ISSN: 1311-1728 (printed version); ISSN: 1314-8060 (on-line version)

[2] M.A.R. Sharif, Laminar mixed convection in shallow inclined driven cavities with hot moving lid on top and cooled from bottom, Appl. Therm. Eng. 27 (2007) 1036-1042.

[3] A.K. Prasad, J.R. Koseff, Combined forced and natural convection heat transfer in a deep lid-driven cavity flow, Int. J. Heat Fluid Flow 17 (1996) 460-467.DOI: 10.1016/0142-727X(96)00054-9.

[4] B. Ghasemi, S.M. Aminossadati, Comparison of mixed convection in a square cavity with an oscillating versus a constant velocity wall, Numer. Heat Transfer A 54 (2008) 726-743. DOI:10.1080/10407780802338959.

[5] H.F.Oztop, I.Dagtekin, Mixed convection in two-sided lid-driven differently heated square cavity, Int. J. Heat Mass Trans., 47, (2004) 1761-1769. DOI:10.1016/ j.ijheatmasstransfer.2003.10.016.

[6] A.J. Chamkha, Hydromagnetic combined convection flow in a vertical lid-driven cavity with internal heat generation or absorption, Numer. Heat Transfer A 41 (2002) 529-546. DOI: doi.org/10.1080/104077802753570356.

[7] Tanmay Basak, S. Roy, Pawan Kumar Sharma, I. Pop, Analysis of mixed convection flows within a square cavitywith uniform and non-uniform heating of bottom wall, Int. J. Therm. Sci. 48 (2009) 891-912. DOI: 10.1016/j.ijthermalsci.2008.08.003.

[8] G. Guo, M.A.R. Sharif, mixed convection in rectangular cavities at various aspect ratios with moving isothermal sidewalls and constant flux heat source on the bottom wall, Int. J. Therm. Sci. 43 (2004) 465-475.DOI:10.1016/j.ijthermalsci.2003.08.008.

[9] H. Masuda, A. Ebata, K.Teramae and N.Hishinuma, Alteration of thermal conductivity and viscosity of liquid by dispersing ultra-fine particles (dispersion of $Al_2O_3, SiO_2 and TiOO_2$ ultra-fine particles), NetsuBussei (in Japanese), 7 (4) (1993) 227-233.DOI: 10.2963/jjtp.7.227.

[10] S.U.S. Choi, Enhancing thermal conductivity of fluids with nanoparticles, in: Proceedings of the 1995 ASME International Mechanical Engineering Congress and Exposition ASME, New York (1995) 99-105.

[11] J.C. Maxwell, A treatise on electricity and magnetism. second ed, Oxford University Press, Cambridge (1904) 435-441.

[12] S. Kumar, S.K. Prasad, J. Banerjee, Analysis of flow and thermal field in nanofluid using a single phase thermal dispersion model, Appl. Math. Model. 34 (2010) 573-592. DOI: 10.1016/j.apm.2009.06.026.

[13] M. Muthtamilselvan, P. Kandaswamy, J. Lee, Heat transfer enhancement of copperwater nanofluids in a lid-driven cavity, Commu. Nonlinear science and Numerical Simulation, 15 (2010) 1501-1510. DOI: 10.1016/j.cnsns.2009.06.015.

[14] A.A. AbbasianArani, S. MazroueiSebdani, M. Mahmoodi, A. Ardeshiri, M. Aliakbari, Numerical study of mixed convection flow in a lid-driven cavity with sinusoidal heating on sidewalls using nanofluid, Super. Micro. 51 (2012) 893-911. DOI: 10.1016/j.spmi.2012.02.015.

Volume 38 No. 1s, 2025

ISSN: 1311-1728 (printed version); ISSN: 1314-8060 (on-line version)

[15] D.S. Bondarenko, M.A. Sheremet, H.F. Oztop, N. Abu-Hamdeh, Mixed convection heat transfer of a nanofluid in a lid-driven enclosure with two adherent porous blocks. J. Ther. Analy. Calori., 135(2), (2019), 1095-1105. DOI: 10.1007/s10973-018-7455-9.

[16] E.V. Shulepova, M.A. Sheremet, H.F. Oztop, N. Abu-Hamdeh, Mixed convec-tion-radiation in lid-driven cavities with nanofluids and time-dependent heatgenerating body. J. Ther. Analy. Calori., 146(2), (2021), 725-738. DOI:10.1007/s10973-020-10003-7.

[17] M.M. Rashidi, M. Sadri, M.A. Sheremet, Numerical simulation of hybrid nanofluid mixed convection in a lid-driven square cavity with magnetic field using high-order compact scheme. Nanomat., 11(9), (2021), 2250. DOI: 10.3390/nano11092250.

[18] A. I. Alsabery, M. Vaezi, T. Tayebi, I. Hashim, M. Ghalambaz, A.J. Chamkha, Nanofluid mixed convection inside wavy cavity with heat source: A non-homogeneous study. Case Studies in Ther. Eng, 34, (2022), 102049. DOI:10.1016/j.csite.2022.102049.

[19] W. Yu, S.U.S. Choi, The role of inter facial layers in the enhanced thermal conductivity of nanofluids: a renovated Maxwell model, J. Nano. Res. 5 (2003) 167-171. DOI: 10.1023/A:1024438603801.

[20] S.V. Patankar, Numerical Heat Transfer and Fluid Flow, Hemisphere, Washington, DC (1980).

[21] T. Hayase, J.A.C. Humphrey, R. Grief, A consistently formulated QUICK scheme for fast and stable convergence using finite-volume iterative procedures, J. Compt. Phys. 98 (1992) 108-118. DOI:10.1016/0021-9991(92)90177-Z.

[22] R. Iwatsu, J.M. Hyun, K. Kuwahara, Mixed convection in a driven cavity with a stable vertical temperature gradient, Int. J. Heat Mass Transfer 36 (1993) 16011608. DOI: 10.1016/S0017-9310(05)80069-9.

[23] A. Arefmanesh, M. Mahmoodi, Effects of uncertainties of viscosity models for Al_2O_3 -water nanofluid on mixed convection numerical simulations, Int. J. Therm. Sci. 50 (2011) 1706-1719. DOI: 10.1016/j.ijthermalsci.2011.04.007.

Received: July 18, 2025